IEEE Access
Multidisciplinary ⋮ Rapid Review ⋮ Open Access Journal

Received July 25, 2020, accepted August 5, 2020, date of publication August 10, 2020, date of current version August 21, 2020.

Digital Object Identifier 10.1109/ACCESS.2020.3015282

Investigation of Semi-Rigid Coaxial Test Probes as RF Injection Devices for Immunity Tests at PCB Level

XINGLONG WU[1], (Graduate Student Member, IEEE),
FLAVIA GRASSI[1], (Senior Member, IEEE),
GIORDANO SPADACINI[1], (Senior Member, IEEE),
SERGIO AMEDEO PIGNARI[1], (Fellow, IEEE),
UMBERTO PAOLETTI[2], (Senior Member, IEEE),
AND ISAO HODA[2], (Member, IEEE)

[1]Department of Electronics, Information, and Bioengineering, Politecnico di Milano, 20133 Milan, Italy
[2]Center for Technology Innovation – Production Engineering, Hitachi, Ltd. Research & Development Group, Yokohama 244-0817, Japan

Corresponding author: Flavia Grassi (flavia.grassi@polimi.it)

ABSTRACT This work investigates the performance of RF immunity procedures exploiting semi-rigid coaxial test probes as coupling devices to inject continuous wave (CW) RF power into the outlets of Integrated Circuits (ICs). Two solutions are presented, both offering the advantage with respect to the traditional direct power injection method, to run the test without removing the IC from its actual PCB. The first procedure resorts to near-field coupling to inject the noise into an interconnecting trace. The second procedure requires metallic contact between the probe tip and the injection point (e.g., a via or an IC pin). Specific figures of merit, such as coupling and power efficiency, test repeatability and intrusiveness, sensitivity to setup parameters and lateral spatial resolution, are introduced and used to ascertain the effectiveness of the proposed procedures. To this end, both numerical simulations and measurements were carried out on several PCBs. Feasibility of the proposed immunity procedures is eventually proven by an application example, involving a thermal sensor as device under test.

INDEX TERMS Direct power injection, microstrip line, near-field probe, radiated immunity, radio frequency.

I. INTRODUCTION

The growing complexity of electronic systems requires the development of novel test procedures aimed at assessing the immunity of specific components and sub-systems mounted on printed circuit boards (PCBs). In this framework, direct power injection (DPI) [1] is a commonly used technique to assess the electromagnetic (EM) susceptibility of integrated circuits (ICs). This method requires direct physical connection between the injection device and the pin(s) under test, and allows the injection of continuous wave (CW) RF disturbance into the IC under test through specific pin(s). However, in order to provide a controlled injection path, DPI testing requires the IC to be mounted on a special test PCB.

The associate editor coordinating the review of this manuscript and approving it for publication was Andrei Muller.

In the same framework, near-field scanning has recently gained increasing attention for EM-field measurement. This technique allows mapping the EM-field distribution on top of a PCB so to identify ICs possibly responsible for interference. Moreover, the obtained EM-field maps can be post-processed, e.g., reconstructed by equivalent surface dipoles, and then used as the interference source for numerical simulation of complex systems, [2]. To this end, the electric and/or magnetic field distribution above the circuit under test is measured by the use of near-field probes (e.g., semi-rigid coaxial cables or PCB-based probes [3]–[8]) assuring high sensitivity to local EM field components and spatial resolution. These characteristics make these probes attractive also as injection devices for immunity testing. Indeed, resorting to near-field probes for noise injection is definitely less intrusive than DPI, since it is not necessary to put injection devices in metallic contact with the pin/trace under test. Moreover, the test can

be executed keeping the IC under test mounted on the actual PCB used in real applications.

The use of near-field probes for investigating PCB susceptibility to EM disturbance is reported in [9]. Several applications of near-field probes for detecting EM-susceptible areas in chips are presented in [10] and [11]. In [12] and [13], near-field probes are used to identify PCB areas susceptible to Electrostatic Discharge (ESD). Further examples of immunity verifications through near-field probes are presented in [14] and [15], where the EM susceptibility of an operational amplifier and a logic circuit, respectively, was detected by the use of near-field magnetic probes.

Although the absence of physical connection between the injection device and the trace/pin under test is definitely attractive, immunity procedures involving non-contact testing have two main drawbacks compared to contact testing. First, the coupling effectiveness, as the amount of RF power transferred from the generator to the circuit under test, is lower than that for contact tests. Hence, a non-contact test generally requires a larger amount of forward power as well as injection devices with higher power rating than directly injected testing. Second, geometrical and electrical parameters may significantly influence the transfer function between the probe and the trace under test, leading to issues in terms of test repeatability and reliability. Hence, it is deserved to investigate the alternative solution, in which near-field probes are used to inject RF power through metallic contact with the pin under test. This option may significantly mitigate the aforesaid effects due to geometrical parameters. With respect to DPI, on the one hand the contact test is still intrusive (which can be anyway accepted, depending on the specific test case), on the other hand it offers the advantage that removing the IC from the actual PCB is no longer required.

In this work, the performance of near-field probes originally designed for electric-field measurement when used as injection devices for immunity verification at PCB level is experimentally and numerically investigated in the frequency range from 30 MHz up to 6 GHz. Particularly, in order to satisfy typical requirements in terms of injected power, the use of semi-rigid coaxial cables with tip characteristics optimized for the specific purpose at hand is proposed. For both contact and non-contact testing, the coupling performance of such probes is systematically investigated by measurements and numerical simulations. This allows the effects of geometrical/electrical parameters of the probe and of the circuit under test on RF power transfer to be estimated, as well as the performance of the two proposed immunity techniques to be compared in terms of lateral spatial resolution, repeatability, and intrusiveness. The feasibility of the proposed injection techniques is proven by an example of test execution which is aimed at assessing the RF immunity of a thermal sensor.

The manuscript is organized as follows. In Section II the desired characteristics of the immunity tests, as well as the probes under consideration are introduced. Injection performance of such probes is investigated in Section III, where a specific probe design (involving a semi-rigid coaxial cable) is proposed. Sections IV and V are devoted at analyzing the intrusiveness and repeatability of the non-contact test procedure, respectively. In Section VI, both the proposed procedures are used to test the immunity of a thermal sensor. Finally, conclusions are drawn in Section VII.

II. CHARACTERISTICS OF IMMUNITY TESTS AND INJECTION PROBES

Electric near-field probes are common tools for near-field measurement on ICs and PCBs, and will be hereinafter considered as candidate coupling devices for susceptibility verification. The figures of merit considered to ascertain the suitability of a specific near-field probe for immunity testing are the probe coupling coefficient, its lateral spatial resolution, and also the maximum forward power the probe can withstand without damage. Indeed, the coupling coefficient and the maximum forward power determine the probe effectiveness in injecting a required level of RF noise into the IC under test. Conversely, the probe lateral spatial resolution is strictly related to test selectivity, that is to the ability to inject RF noise on the specific trace/pin under test only, with negligible interference to adjacent traces/pins.

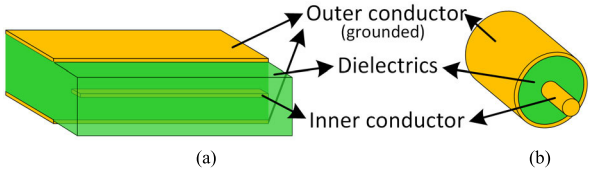

FIGURE 1. Principle drawing of typical probe tips: (a) PCB-based; (b) coaxial cables.

To the best of the Authors' knowledge, available electric near-field probes possibly suitable for EM susceptibility investigation can be grouped into two main categories: (a) PCB-based probes (see Fig. 1(a)) [5], [8]; and (b) semi-rigid coaxial cable probes (see Fig. 1(b)) [3], [13], [15], [16]. Probes belonging to the former group exhibit geometries carefully designed to optimize coupling and field directivity performance. However, the use of a PCB inherently limits the maximum power the probe can withstand without damage. Hence, the vast majority of PCB-based near-field probes available on the market are intended to be used as field sensors (i.e., monitor probes), and their use for RF power injection is generally discouraged by manufacturers (at least for injected forward power levels above 5 W).

To overcome this limitation, semi-rigid coaxial test probe assemblies, each of which has an exposed inner conductor on one end of the cable, are considered in this work. Indeed, such an alternative solution allows reaching power levels adequate for IC testing, yet it is very simple. As an example, Table 1 lists the maximum (forward) power allowed by the three semi-rigid coaxial cables exploited in this work. For SMA connectors, a maximum power in the order of 150 W can be considered in the frequency range of interest.

TABLE 1. Maximum power of semi-rigid coaxial cables [17].

	RG405	PE047	PE034
Inner conductor dimension	Φ0.51 mm	Φ0.28 mm	Φ0.20 mm
Maximum power (<1 GHz)	130 W	32 W	10 W
Maximum power (<10 GHz)	35 W	9 W	3.1 W

III. INJECTION PERFORMANCE: COUPLING COEFFICIENT AND LATERAL SPATIAL RESOLUTION

In this Section, the impact of geometrical characteristics on the injection performance of electric near-field probes based on the use of semi-rigid coaxial cables is investigated with reference to the figures of merit introduced in the previous section. To this end, three semi-rigid coaxial probes, which can generate electric field in the direction perpendicular to the PCB under test (i.e., z-direction), were fabricated. The performance of these semi-rigid coaxial probes was investigated by using 3D numerical simulations and Vector Network Analyzer (VNA) measurements.

In both measurement and simulation, each of the probes under analysis was mounted onto some microstrip structures, involving several adjacent lines equipped with SMA terminal connectors. The S-parameters at each pair of available ports were measured/simulated. Among them, the transmission coefficient from the probe input port to one of the two terminations of the trace under test represents a measure of the probe injection performance, and will be hereinafter denoted as *probe coupling coefficient*, S_{coup}. The transmission coefficient from the probe input port to the terminations of one of the nearby traces (hereinafter denoted as *crosstalk*, S_{XT}) represents a measure of the probe lateral spatial resolution.

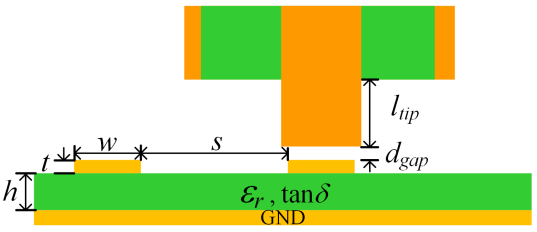

FIGURE 2. Cross section of the simulation setup exploited to investigate the influence of the probe-tip length on coupling performance.

A. INFLUENCE OF THE TIP LENGTH

The influence of the tip length on the coupling performance of coaxial near-field probes is investigated using a specific set of simulations carried out by the numerical solver Ansys HFSS. Fig. 2 shows the cross section of the setup implemented for numerical simulation. The setup involves a double-layer PCB with two microstrip copper traces printed on the top side with the following geometrical and electrical characteristics: substrate thickness $h = 70$ μm, substrate relative permittivity $\varepsilon_r = 3.4$, substrate dissipation factor tan$\delta = 0.001$, trace thickness $t = 18$ μm, trace width $w = 0.15$ mm, trace separation $s = 2$ mm, trace length $L = 149$ mm. The probe is placed 0.02 mm (d_{gap}) above the trace midpoint. The coaxial probe is realized by an 11.75 mm long RG405 cable, with tip length varying from 5 mm to 0 mm (i.e., flush cut tip).

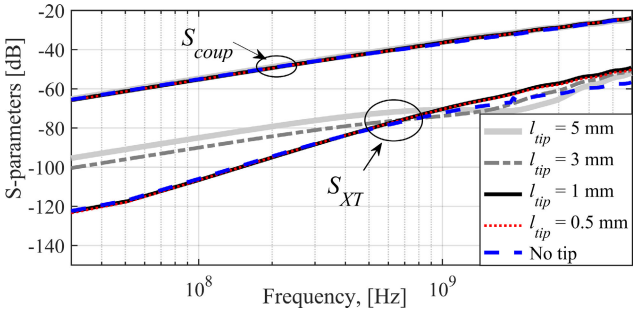

FIGURE 3. Coupling and crosstalk coefficients for different tip lengths (coaxial cable RG405).

The simulation results shown in Fig. 3 indicate that a) the tip length does not affect the coupling coefficient itself; b) on condition the length of the coaxial tip is kept short, that is from 0 up to 1 mm in this case, comparable crosstalk levels are observed. For larger tip lengths, significantly higher (∼20 dB) crosstalk levels are observed in the low frequency interval.

On the basis of the above results, semi-rigid coaxial test probes with 1 mm tips will be hereinafter considered as a trade-off solution to reduce crosstalk on the one hand and to enhance positioning resolution on the other. As a matter of fact, eliminating the tip would pose possible issues in terms of probe positioning, especially in densely-populated PCBs (e.g., risk of inadvertently putting the probe tip on wrong traces and/or the probe shield in contact with nearby traces).

B. INFLUENCE OF THE PROBE DIAMETER

In this Subsection, the influence of the probe-tip diameter is investigated in combination with PCB-trace separation by a set of VNA measurements with Keysight E5071C.

A picture of the experimental setup along with a principle drawing of its cross section is shown in Fig. 4(a). The exploited PCB involves two sets of three parallel traces (named "PL1" and "PL2") printed on the top layer with nominal geometrical and electrical characteristics as follows: copper thickness $t = 35$ μm, substrate material FR4 R1551 (max. $\varepsilon_r = 4.7$ @ 1 GHz, max. tan$\delta = 0.011$ @ 1 GHz), substrate thickness $h = 80$ μm, trace width $w = 0.15$ mm, trace separation $s = 0.5$ mm (PL1) and $s = 0.15$ mm (PL2), trace length $L = 134$ mm. The PCB is protected by a solder mask with nominal thickness $t_{mask} = 30$ μm, realized in PSR-4000 MP ($\varepsilon_r = 4.7$ @ 1 MHz).

For measurement, the probes are placed on top of the inner trace of PL1 and PL2 at midpoint. Measurements were carried out in the frequency interval from 30 MHz up to 6 GHz by a four-port VNA Keysight E5071C. The results were also compared versus those obtained by using a commercial

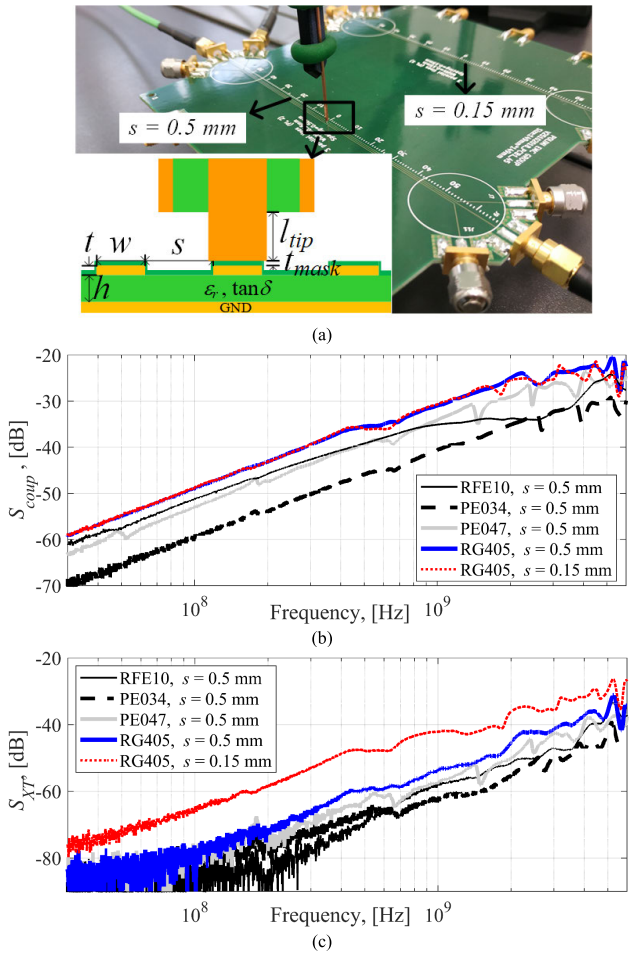

FIGURE 4. Impact of probe dimensions and trace separation: (a) PCB under test; (b) measured coupling coefficient; (c) measured crosstalk coefficient.

PCB-based probe (Langer RF E10, [18]). The measured coupling and crosstalk coefficients are shown in Fig. 4(b) and Fig. 4(c), respectively.

For all probes, measurement data confirm that the highest coupling coefficient is obtained by the use of the semi-rigid coaxial cable with the largest diameter (i.e., RG-405). For coaxial probes, the coupling coefficient linearly increases with a slope of +20 dB/dec up to 2 GHz, reaching maximum values on the order of –20 dB at the highest frequencies of interest (i.e., 5∼6 GHz). This behavior indicates that the coupling effectiveness is mainly governed by the coupling capacitance between the probe and trace under test, at least in the frequency range up to 2 GHz.

Crosstalk measurements were used to investigate probe performance in terms of lateral spatial resolution. To this end, the minimum difference between the coupling coefficient and the crosstalk coefficient measured at the terminations of lateral traces, i.e.,

$$\Delta dB_{min} = \min\left\{20\log_{10}|S_{coup}(f)/S_{XT}(f)|\right\} \qquad (1)$$

is considered to provide a quantitative indication of lateral spatial resolution.

TABLE 2. Lateral spatial resolution of near-field probes.

ΔdB_{mm}		RFE10	RG405	PE047	PE034
PL1 (s = 0.5 mm)	30 MHz~3 GHz	20.1	19.1	17.0	9.9
	3 GHz~6 GHz	9.23	10.7	10.9	10.1
PL2 (s = 0.15 mm)	30 MHz~3 GHz	16.6	13.4	14.0	10.1
	3 GHz~6 GHz	0.6	2.8	4.0	0.9

The results obtained are collected in Table 2. As expected, for smaller trace separation, higher crosstalk and lower ΔdB_{min} values are obtained. The near-field probe RFE10 assures the best lateral spatial resolution within the suggested frequency interval from 30 MHz up to 3 GHz. Although smaller, the lateral spatial resolution gained by the RG405 probe is anyway acceptable, since it assures a minimum difference of 13.4 dB up to 3 GHz even for 0.15 mm trace separation. As a general rule, coaxial probes with smaller tips assure lower crosstalk to adjacent traces, yet at the price of lower coupling coefficient. Hence, the corresponding lateral spatial resolution, ΔdB_{min}, does not exhibit significant improvement. Indeed, the RG405 probe, which assures the highest coupling coefficient (see Fig. 4(b)), provides similar lateral spatial resolution as the PE047 probe. For this reason, the near-field probe realized by the coaxial-cable RG405 with 1 mm tip will be hereafter considered.

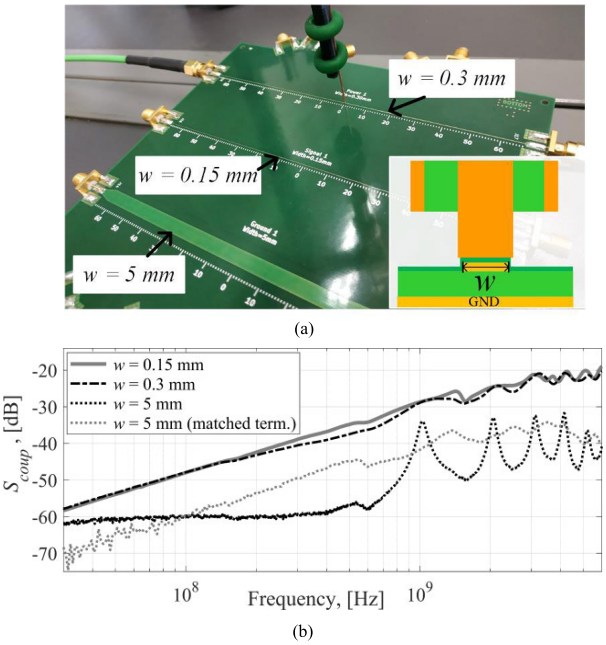

FIGURE 5. Influence of geometrical/electrical characteristics of the trace under test: (a) test setup; (b) measured coupling coefficients (RG405 coaxial probe).

C. INFLUENCE OF THE GEOMETRICAL/ELECTRICAL CHARACTERISTICS OF THE TRACE UNDER TEST

To investigate the influence of geometrical/electrical characteristics of the trace under test on near-field injection, three

single traces with different width and terminated in 50 Ω loads were setup, as shown in Fig. 5(a). PCB characteristics are the same as those in Fig. 4. The widths of the three traces are equal to 0.15, 0.3, and 5 mm.

For all semi-rigid coaxial probes, measurements of the coupling coefficient were carried out by positioning the probe at the trace midpoint. For the sake of brevity, only results obtained for the semi-rigid coaxial probe RG405 are presented in Fig. 5(b), since for the other probes similar conclusions can be drawn. Namely, the comparison in Fig. 5(b) proves that the trace width does not significantly influence the coupling coefficient as long as the interconnection under test is not significantly wider than the probe cross-section diameter and is able to effectively transmit signals in the frequency interval of interest. As a matter of fact, the coupling coefficients measured on the two traces with width $w = 0.15$ mm and $w = 0.3$ mm (whose characteristic impedances are 45 Ω and 29 Ω, respectively) do not exhibit appreciable differences, although the width of the second trace is twice the width of the first one. Conversely, a significant decrease in the coupling coefficient is observed for the third line. This reduction can be ascribed to the combined effect of spurious coupling between the probe shield and the trace under test and mismatch at trace terminals. Concerning spurious coupling between the probe shield and the trace under test, this can be appreciated by looking at the dotted gray line in Fig. 5(b), which was obtained by post-processing the original coupling coefficient (dotted black line in Fig. 5(b)) with the objective to de-embed the effects introduced by the 50 Ω connectors and to enforce matching at the trace terminals. Concerning mismatch, the actual trace characteristic impedance, 2.6 Ω, is very far from the 50 Ω termination impedance. Therefore, transmission effectiveness of such an interconnection is very poor in the frequency range of interest. On the other hand, mismatch may occur in practice. Consequently, the actual noise entering the pin of the IC under test is low except at resonance frequencies. This reflects the actual propagation properties of a real PCB and marks a point in favor of the proposed method with respect to DPI (involving a special test PCB) which inevitably modifies susceptibility properties of the actual working environment of the IC under test.

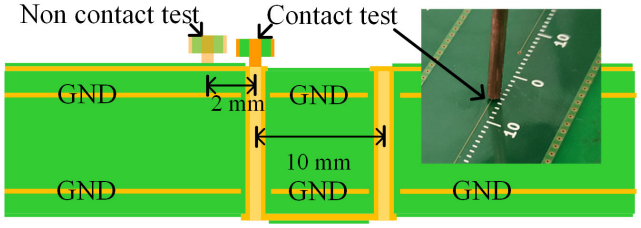

FIGURE 6. Cross-sectional view of the U-type trace exploited to investigate test intrusiveness.

IV. TEST INTRUSIVENESS

To investigate test intrusiveness, transmission and reflection coefficients at the ports of the trace under test are measured in the presence and in the absence of the coaxial probe RG405. To investigate the different performance of the contact and non-contact tests, a U-type trace (see Fig. 6) with trace width $w = 0.15$ mm was printed on a PCB with geometrical/electrical characteristics similar to those exploited in the previous examples. The obtained reflection and transmission coefficients are plotted in Fig. 7(a) and (b), respectively. The comparison confirms the non-intrusiveness of the test carried out with the probe not in metallic contact with the trace under test. Conversely, an appreciable degradation of performance (i.e., a decrease in the transmission coefficient of 0.5∼1.5 dB, as well as a general increase of the reflection coefficient) is observed when the probe tip is put in direct contact with the via hole.

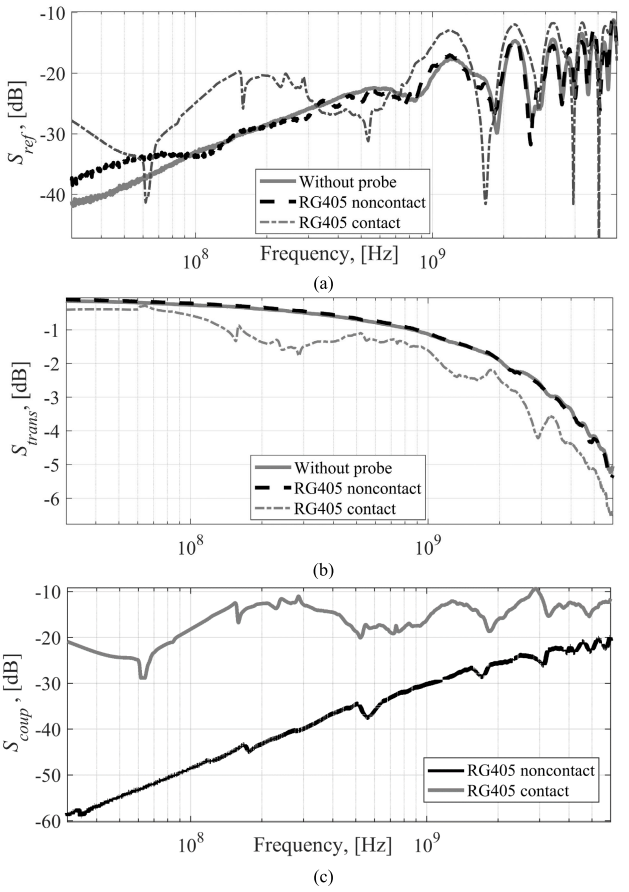

FIGURE 7. Test intrusiveness (see setup in Fig. 6): (a) reflection and (b) transmission coefficients of the trace under test; (c) coupling coefficient. between the probe and one termination of the trace under test.

Such an increased test intrusiveness is anyway compensated by the significantly larger coupling coefficient that can be obtained, by putting the probe in metallic contact with the trace under test. This is shown in Fig. 7(c), where the coupling coefficients measured with the probe in contact and not in contact with the trace under test are compared. Although for contact testing, the low-frequency behavior is non-negligibly affected by the lack of connection between the probe shield and the PCB ground plane, the comparison

in Fig. 7(c) indicates that the coupling effectiveness is anyway significantly improved when the probe tip is in metallic contact with the trace under test.

V. TEST REPEATABILITY

Another important characteristic to qualify the reliability of an immunity test is its repeatability. This issue is of major concern for the non-contact test rather than for the contact test, and it will be thoroughly investigated in this Section by means of specific measurements, aimed at evaluating the sensitivity of test outcomes to probe positioning.

A. SYSTEMATIC INVESTIGATION OF TEST SENSITIVITY TO PROBE-TO-TRACE MISALIGNMENT AND DISTANCE

In this Subsection, the influence of probe positioning with respect to the trace under test is systematically investigated by making use of an automatic scan system (EVM-200).

Measurements of the probe-to-trace coupling coefficient were carried out with a VNA, by mounting the coaxial RG405 probe on top of the single lines in Fig. 5. With reference to the principle drawing in Fig. 8(a), the test was carried out according to the following procedure. To set the starting point, the probe was initially positioned approximately at the center of the trace width (red dot in Fig. 8(a)), then it was moved out of the trace by 1 mm (blue dot in Fig. 8(a)). A specific height, i.e., probe-to-trace distance d, was then set. For such an height, 21 points, separated by a 0.1 mm step, were scanned along the dot black line in Fig. 8(a) within a $L_{test} = 2$ mm interval. The experiment was repeated for different tip-to-trace distances. For the trace with width $w = 0.3$ mm, examples of results are shown in Fig. 8. Similar results, here omitted for the sake of brevity, were obtained for the other traces in Fig. 5.

The 3D plot in Fig. 8(b) shows the sensitivity of the coupling coefficient for probe-to-trace distance $d = 0.1$ mm as function of horizontal position and frequency. The highest coupling is observed when the probe is exactly placed in the middle of the trace under test. For frequencies below 1 GHz (see Fig. 8(c)), the coupling coefficient progressively decreases by moving the probe by the sides of the trace. Conversely, for frequencies above 1 GHz, the coupling coefficient exhibits local minima exactly at the borders of the trace under test (see in Fig. 8(d)). Then, it exhibits a nearly constant value by the sides of the trace.

As far as sensitivity to vertical positioning is concerned, a pronounced decrease in the coupling is observed when the probe-to-trace distance, d, decreases. This significantly impacts also on sensitivity to horizontal positioning. As a matter of fact, Fig. 8(b) and (c) show that the smaller the vertical distance d, the larger are the differences observed in the coupling coefficient for the same horizontal shifts.

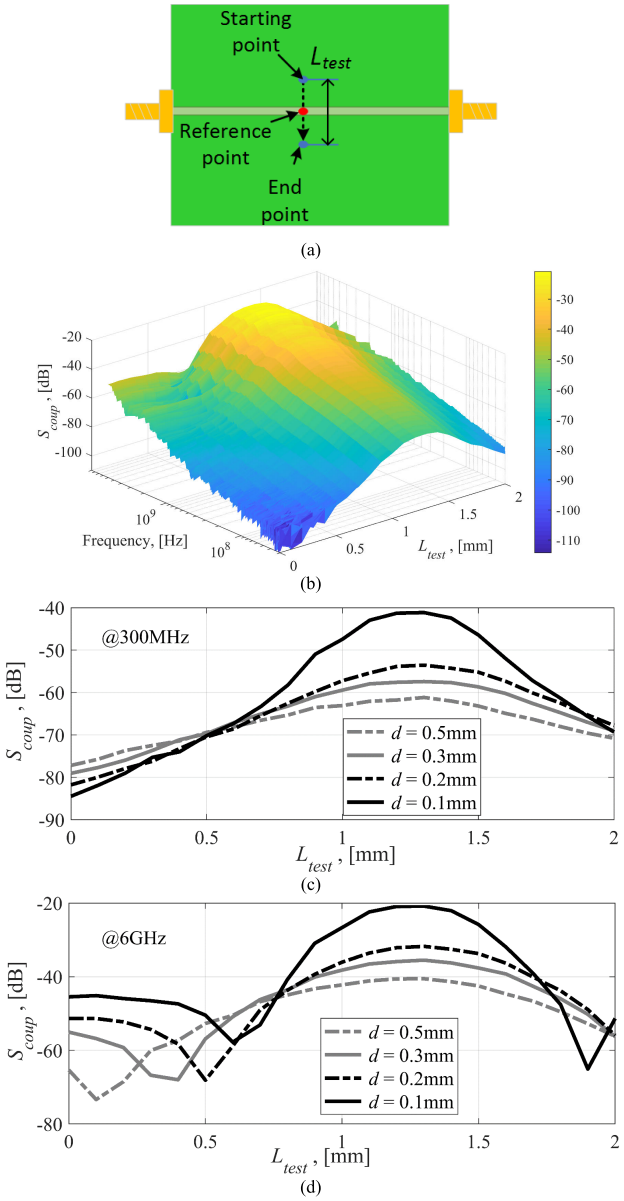

FIGURE 8. Sensitivity of the coupling coefficient to probe-to-trace misalignment and distance. (a) Principle drawing of the automatic test (b) 3D plot obtained for d = 0.1 mm. Coupling coefficient for different probe-to-trace distances at (c) 300 MHz, and (d) 6 GHz.

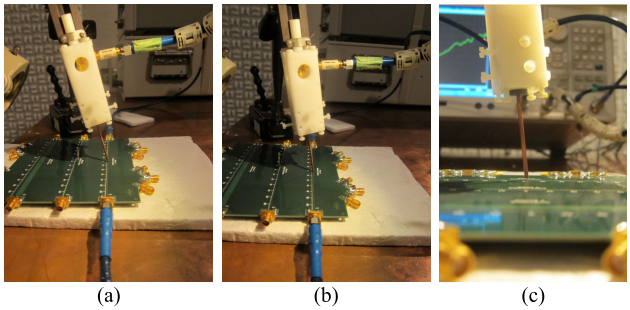

FIGURE 9. Sensitivity to probe rotation around the horizontal axis: (a) heavy tilt; (b) medium tilt; (c) medium tilt in the trace direction.

B. SENSITIVITY TO PROBE ROTATION

To investigate the sensitivity of the coupling coefficient to probe rotation with respect to the horizontal axis, the test setup in Fig. 9 is exploited, which involves the coaxial probe RG405 mounted on the solder mask of the single-ended trace with width $w = 0.3$ mm (see Sec. III for further details on

PCB characteristics). The coupling coefficients measured for different rotation angles are plotted in Fig. 10. The comparison shows that probe rotation causes a decrease in the coupling coefficient, which, even in the worst-case condition here considered (see Fig. 9(a)), does not anyway exceed 5 dB.

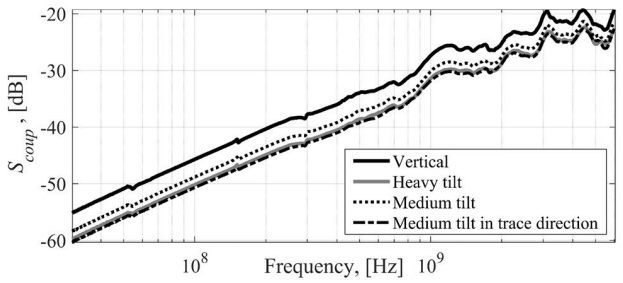

FIGURE 10. Coupling coefficients measured for different rotation angles w.r.t. the vertical axis.

C. UNCERTAINTY DUE TO MANUAL POSITIONING

Based on previous results, it can be expected that the ability of the operator in properly positioning the probe on top of the trace under test may introduce some uncertainty in the evaluation of the RF noise actually injected during the test.

To quantify such an uncertainty, an additional test was carried out, in which three different operators were requested to properly position the coaxial probe RG405 (a manual positioner Cascade Microtech E2654A is used in order to host the probe) on top of the trace under test, by resorting to a magnifier only. Each operator attempted twice, and was prevented from looking at the screen of the VNA to judge in advance the goodness of the achieved positioning. The measured coupling coefficients are plotted in Fig. 11, and show maximum differences on the order of 2 dB.

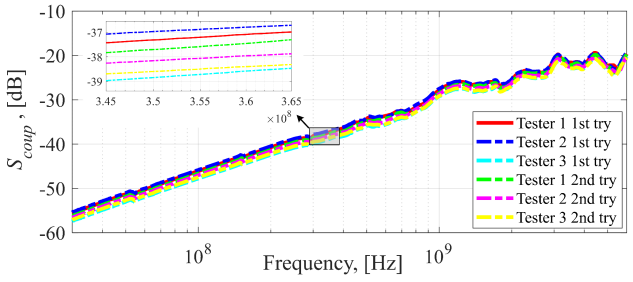

FIGURE 11. Experimental blind assessment of sensitivity to tester.

VI. EXAMPLE OF TEST EXECUTION: IMMUNITY TEST OF A THERMAL SENSOR

In this Section, feasibility and effectiveness of the proposed immunity test are evaluated by an explicative example of test execution, aimed at assessing the susceptibility of a thermal sensor. Particularly, the test was carried out with the probe both in metallic contact and not in contact with the injection trace/pin on the PCB to compare the performance of the two test implementations, with particular focus on the forward power required to induce RF susceptibility in the sensor under test.

A. DESCRIPTION OF DEVICE UNDER TEST

The device under test is an isolated temperature sensor. To detect temperature variation, the sensor uses a power module comprising diodes, whose switching characteristics are temperature sensitive. An external IC allows detecting temperature variations (ΔT) in terms of variation of the duty cycle δ of the output PWM signal.

Namely, the measured temperature T (in °C) and the duty cycle δ (in percentage) are related by the empirical expression:

$$T = -6.526 \times \delta + T_0 \tag{2}$$

where T_0 represents a reference temperature (i.e., room temperature) to be calibrated at the beginning of the test.

B. DESCRIPTION OF THE TEST SETUP

A principle diagram of the test bench set up to investigate the immunity of the thermal sensor under analysis is shown in Fig. 12. The test bench was set up onto the metallic ground plane above a wooden table in an anechoic chamber.

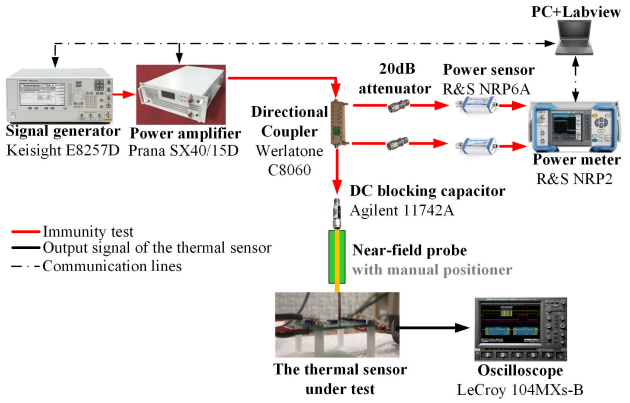

FIGURE 12. Principle diagram of the test bench setup to assess the immunity of the thermal sensor by the semi-rigid coaxial probe RG-405.

The signal generator (Keisight E8257D), the power amplifier (Prana SX40/15D, 800 MHz∼6 GHz), and the power meter (R&S NRP2) are controlled by a Labview routine to provide an automatic frequency sweep. To measure the duty cycle, the IC output signal was read by an oscilloscope placed in the chamber control room and connected with the IC through optical fibers.

Moreover, the setup comprises a directional coupler Werlatone C8060 (200 MHz-6 GHz), 20 dB attenuators, and a DC blocking capacitor (Agilent 11742A) connected at the input port of the coaxial probe. An infrared camera (FLIR i3) was used with the twofold aim of (a) calibrating the temperature sensor at the beginning of the test [so to evaluate the reference temperature T_0 in (2)]; and (b) monitoring the

actual temperature of the injection pin to assess whether the observed increase in the measured temperature is due to RF interference or due to the actual temperature increase, as correctly detected by the sensor.

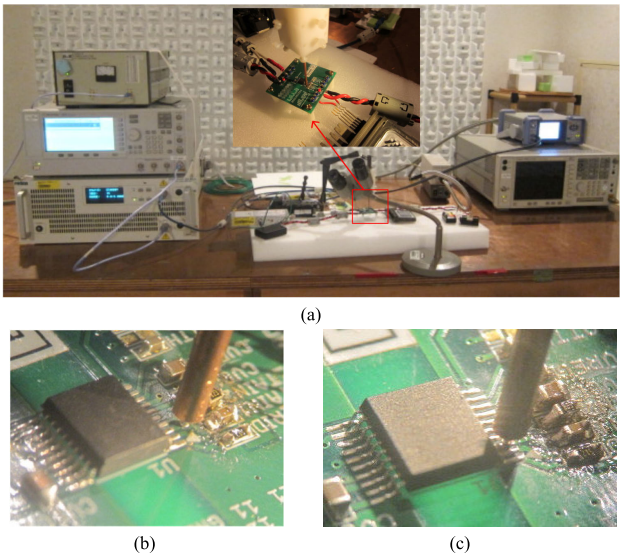

FIGURE 13. Pictures of the setup for testing the immunity of the temperature sensor: (a) overall view, and zoomed view, showing probe positioning for (b) non-contact, and (c) contact testing.

An overall view of the test setup is shown in Fig. 13(a). For non-contact testing, the semi-rigid coaxial probe RG-405 was placed on the trace (protected by the solder mask) connected to the (functional) input pin of the sensor, as shown in Fig. 13(b). For contact testing, the probe was put in metallic contact with the input pin of the sensor, as shown in Fig. 13(c).

C. RATIONALE OF THE TEST

Since the thermal sensor under test exhibited a malfunction in the frequency interval around 900 MHz, a first immunity test was run by sweeping the frequency interval from 800 MHz up to 1 GHz. To run the test with a constant power at the input of the probe, the following procedure was adopted to compensate the effects due to the nonlinear response of the RF power amplifier as well as variation of the equivalent impedance seen from the outlets of the signal generator.

1) Given the desired injected power P_{exp}, the frequency-constant value P_{SG} of forward power was set on the signal generator and a preliminary sweep in the frequency range from 800 MHz up to 1 GHz was run with step 10 MHz (21 frequency points).

2) The actual injected power was then calculated, frequency by frequency, starting from the forward P_F and reflected power P_R measured by the power meter as

$$P_{in}(f) = G_{atten}\,[P_F(f) - P_R(f)] \tag{3}$$

where $G_{atten} = 10000$ denotes the total attenuation due to the directional coupler (20 dB) and the attenuator at the input of the power sensors (20 dB).

3) The difference between the expected and actual injected power $DIFF(f) = P_{exp} - P_{in}(f)$ allows evaluating the forward power to be set at the signal generator

$$P_{SGnew}(f) = P_{SG} + DIFF(f) \tag{4}$$

which assures a constant-valued power, P_{exp}, at the input of the probe. More specifically, the power at the probe input was kept constant to the values 22 dBm and 35 dBm for the contact and non-contact test, respectively. For two frequency points only, *posteriori* adjustments (repeat step 2 and 3) were required in the case of the non-contact test, due to the amplifier non-linear behavior.

D. TEST RESULTS

Post-processing the acquired duty cycle and power readings according to (2) and (3) yielded the results plotted in Fig. 14. The plots of the injected power (see right axis) confirm the effectiveness of the adopted procedure in maintaining the actual power at the probe input constant over frequency.

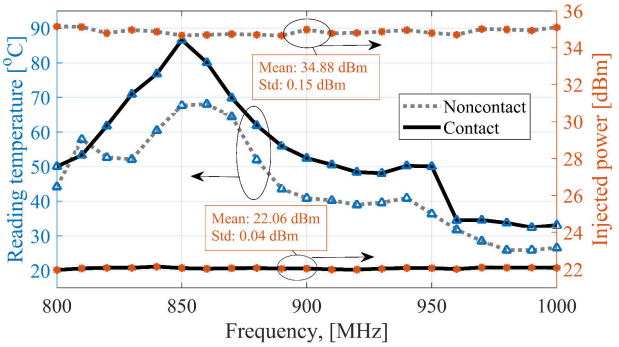

FIGURE 14. Temperature read by the sensor (left axis) as function of frequency for a constant power at the probe input (right axis): (a) non-contact test (input power: 35 dBm); (b) contact test (input power: 22 dBm).

The temperature plots (see left axis) indicate strong RF susceptibility of the IC under test for frequencies around 850∼860 MHz, where the detected temperature exhibits a pronounced peak in spite of the fact that the actual temperature read by the infrared camera was significantly lower, i.e., around 26° C and 31° C (such a variation is due to the increase of the chamber temperature during the test) for the whole duration of the test. After the peak, the temperature detected by the sensor starts decreasing and reaches values consistent with the readings of the infrared camera for frequencies close to 1 GHz. Moreover, discontinuous changes of temperature reading of the sensor were observed at each moment of switching the injection power on/off. These allow it to be concluded that the temperature increase detected by the thermal sensor is the consequence of sensor susceptibility to RF interference for frequencies around 800 MHz and 950 MHz, rather than to an actual increase of the temperature of the power module.

Further investigations were carried out considering three specific frequencies, i.e., 800, 850 and 900 MHz, and by

progressively increasing the power at the output of the signal generator by a step of 1∼2 dB. The obtained results are shown in Fig. 15.

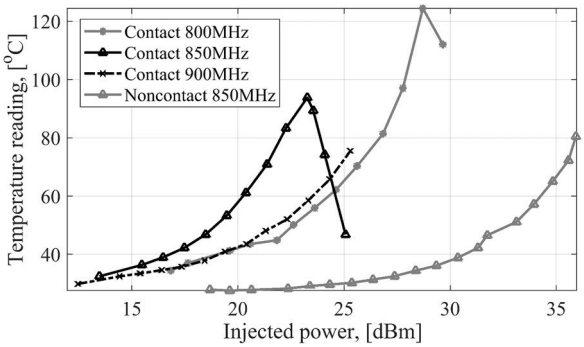

FIGURE 15. Contact vs non-contact test: temperature detected by the thermal sensor as function of power at the probe input at 800 MHz, 850 MHz and 900 MHz.

In the plots for the contact test, it is worth noticing that the read temperature increases for increasing injected power up to a certain limit, after that it starts decreasing due to overflow error of the data. At 850 MHz, this inflection is observed for relatively low value of injected power (around 23.5 dBm), which further confirms the largest RF susceptibility of the sensor for frequencies around 850 MHz.

Concerning the comparison between the two tests, the power required to induce RF susceptibility in the sensor with the probe not in contact is nearly 15 dB larger [see the comparison in Fig. 15, which is also in line with the results obtained at 850 MHz shown in Fig. 7(c)] than the power required when the probe is in metallic contact with the IC pin. Anyway, such a disadvantage in terms of required power is compensated by the non-intrusiveness of the test, which can be a requirement of paramount importance depending on the specific application. In passing, it is worth mentioning that no electrical arcs/breakdowns were observed during the tests.

VII. CONCLUSION

In this work, two test procedures aimed at assessing IC immunity to EM disturbance in the frequency interval from 30 MHz to 6 GHz were introduced, which make use of semi-rigid coaxial cables with suitable characteristics as injection devices. With respect to the traditional DPI technique, both the proposed procedures offer the advantage that the IC under test does not need to be removed from its actual PCB. Thanks to this feature, the proposed procedures are especially beneficial for testing with isolated ICs, to which it is difficult to apply the DPI technique because a multiple grounding strategy is required.

The first procedure (non-contact testing) does not require metallic contact between the probe tip and the circuit under test, since it resorts to near-field coupling for noise injection. This offers a great flexibility in the selection of the injection point (e.g., any interconnecting trace, even if protected by the solder mask, can be used), and assures test non-intrusiveness.

The second procedure (contact testing) requires putting the probe tip in metallic contact with the injection point, which can be a via or the pin of the IC under test. This results in a slight increase in test complexity, since grounding conditions as well as the risk to short adjacent metallic pins should be carefully considered by the operator. Moreover, the test is no longer non-intrusive, since the presence of the probe may exert a non-negligible effect of loading on the trace under test. For instance, in the examples reported in this work a degradation of 0.5 dB∼1.5 dB in the transmission performance of the trace under test was observed in the interval from 30 MHz to 6 GHz. However, with respect to the noncontact procedure, contact testing has significant advantages in terms of coupling efficiency, which directly reflects into a decrease of the power required to execute the test. Likewise for other injection methods (e.g., those based on the Bulk Current Injection (BCI) technique), the proposed procedures do not assure directivity, since the RF noise is injected also into the IC connected at the other termination of the trace under test.

Regarding coupling efficiency, in the example proposed in Section VI, it is shown that at 800-900 MHz the power required to induce susceptibility in the device under test with the probe not in metallic contact is on average 15 dB larger than with the probe in contact. This difference is expected to be even larger at lower frequencies (i.e., for frequencies below 500 MHz) due to the poor effectiveness of near-field coupling at the beginning of the frequency interval under analysis. Regarding test repeatability, a systematic investigation was provided to quantify the sensitivity and expected uncertainty of non-contact testing due to setup parameters and probe positioning. Repeated tests allowed estimating a maximum sensitivity to manual positioning in the order of 2 dB, which is acceptable for immunity testing. The example showed that, by using a single test bench, both contact and non-contact procedures worked well for susceptibility analysis, validating the effectiveness of the proposed two procedures.

REFERENCES

[1] *Integrated Circuits—Measurement of Electromagnetic Immunity—Part 4: Direct RF Power Injection Method*, IEC Standard 62132-4, 2006.

[2] X. Tong, D. W. P. Thomas, A. Nothofer, P. Sewell, and C. Christopoulos, "Modeling electromagnetic emissions from printed circuit boards in closed environments using equivalent dipoles," *IEEE Trans. Electromagn. Compat.*, vol. 52, no. 2, pp. 462–470, May 2010.

[3] Y. Gao and I. Wolff, "Miniature electric near-field probes for measuring 3-D fields in planar microwave circuits," *IEEE Trans. Microw. Theory Techn.*, vol. 46, no. 7, pp. 907–913, Jul. 1998.

[4] J. Shi, M. A. Cracraft, K. P. Slattery, M. Yamaguchi, and R. E. DuBroff, "Calibration and compensation of near-field scan measurements," *IEEE Trans. Electromagn. Compat.*, vol. 47, no. 3, pp. 642–650, Aug. 2005.

[5] H. Funato, "Modeling and analysis of near-field probes and electromagnetic radiation from PCB-chassis structure," Ph.D. dissertation, Dept. Elect. Electron. Eng., Tokyo Metropolitan Univ., Tokyo, Japan, 2014.

[6] D. Baudry, C. Arcambal, A. Louis, B. Mazari, and P. Eudeline, "Applications of the near-field techniques in EMC investigations," *IEEE Trans. Electromagn. Compat.*, vol. 49, no. 4, pp. 805–815, Nov. 2007.

[7] R. Hou, M. Spirito, F. Van Rijs, and L. C. N. de Vreede, "Contactless measurement of absolute voltage waveforms by a passive electric-field probe," *IEEE Microw. Wireless Compon. Lett.*, vol. 26, no. 12, pp. 1008–1010, Dec. 2016.
[8] Z. Yan, W. Liu, J. Wang, D. Su, X. Yan, and J. Fan, "Noncontact wideband current probes with high sensitivity and spatial resolution for noise location on PCB," *IEEE Trans. Instrum. Meas.*, vol. 67, no. 12, pp. 2881–2891, Dec. 2018.
[9] *Integrated Circuits—Measurement of Electromagnetic Immunity—Part 9: Surface Scan Method*, IEC Standard TS 62132-9, 2014.
[10] A. Boyer, S. Benhia, and E. Sicard, "Characterization of electromagnetic susceptibility of integrated circuits using near-field scan," *Electron. Lett.*, vol. 43, no. 1, pp. 15–16, 2007.
[11] A. Boyer, B. Vrignon, J. Shepherd, and M. Cavarroc, "Evaluation of the near-field injection method at integrated circuit level," in *Proc. Int. Symp. Electromagn. Compat.*, Goteborg, Sweden, Sep. 2014, pp. 85–90.
[12] D. Pommerenke, G. Muchaidze, J. Koo, Q. Cai, and J. Min, "Application and limits of IC and PCB scanning methods for immunity analysis," in *Proc. 18th Int. Zurich Symp. Electromagn. Compat.*, Sep. 2007, pp. 83–86.
[13] G. Muchaidze, J. Koo, Q. Cai, T. Li, L. Han, A. Martwick, K. Wang, J. Min, J. L. Drewniak, and D. Pommerenke, "Susceptibility scanning as a failure analysis tool for system-level electrostatic discharge (ESD) problems," *IEEE Trans. Electromagn. Compat.*, vol. 50, no. 2, pp. 268–276, May 2008.
[14] M. Girard, T. Dubois, G. Duchamp, and P. Hoffmann, "EMC susceptibility characterization of an operational amplifier-based circuit combining different technique," in *Proc. Int. Symp. Electromagn. Compat. Eur.*, Wroclaw, Poland, Sep. 2016, pp. 300–305.
[15] T. Dubois, S. Jarrix, A. Penarier, P. Nouvel, D. Gasquet, L. Chusseau, and B. Azais, "Near-field electromagnetic characterization and perturbation of logic circuits," *IEEE Trans. Instrum. Meas.*, vol. 57, no. 11, pp. 2398–2404, Nov. 2008.
[16] A. Durier, S. B. Dhia, and T. Dubois, "Comparison of voltages induced in an electronic equipment during far field and near field normative radiated immunity tests," in *Proc. Int. Symp. Electromagn. Compat. Eur.*, Barcelona, Spain, Sep. 2019, pp. 938–943.
[17] Infinite Electronics International. *RG405, PE047SR and PE034SR*. Accessed: 2019. [Online]. Available: https://www.pasternack.com/standard-semi-rigid-50-ohm-coax-rf-cables-category.aspx
[18] Langer EMV-Technik. *RFE10, Langer RF E10 Probe*. Accessed: 2019. [Online]. Available: https://www.langer-emv.de/en/product/rf-passive-30-mhz-3-ghz/35/rf-e-10-e-field-probe-30-mhz-up-to-3-ghz/10

XINGLONG WU (Graduate Student Member, IEEE) received the double M.Sc. degrees in electrical engineering (EE) from Xi'an Jiaotong University, Xi'an, China, and the Politecnico di Milano, Milan, Italy, in 2015, and the Ph.D. degree *(summa cum laude)* in EE from the Politecnico di Milano, in 2019.

He is currently a Postdoctoral Research Fellow of the Department of Electronics, Information, and Bioengineering, Politecnico di Milano. In March and June 2017, he was a Visiting Scientist at the Department of Information Technology, Electromagnetics Group, Ghent University, Belgium. His research interests include distributed parameter circuit modeling, statistical techniques for electromagnetic compatibility (EMC), and system-level EMC.

FLAVIA GRASSI (Senior Member, IEEE) received the M.Sc. and Ph.D. degrees in electrical engineering from the Politecnico di Milano, Milan, Italy, in 2002 and 2006, respectively.

From 2008 to 2009, she was with the European Space Agency (ESA), ESA/ESTEC, The Netherlands, as a Research Fellow. She is currently an Associate Professor with the Department of Electronics, Information, and Bioengineering, Politecnico di Milano. Her research interests include distributed-parameter circuit modeling, statistical techniques, the characterization of measurement setups for electromagnetic compatibility (EMC) testing (aerospace and automotive sectors), and the application of the powerline communications technology in ac and dc lines.

Dr. Grassi received the International Union of Radio Science (URSI) Young Scientist Award, in 2008, the Best Symposium Paper Award from the APEMC, in 2015 and 2018, the IEEE Young Scientist Award from the Asia–Pacific International Symposium on EMC (APEMC), in 2016, and the IEEE EMC Society Transactions Prize Paper Award, in 2016.

GIORDANO SPADACINI (Senior Member, IEEE) received the M.Sc. and Ph.D. degrees in electrical engineering from the Politecnico di Milano, Italy, in 2001 and 2005, respectively.

He is currently an Associate Professor with the Department of Electronics, Information, and Bioengineering, Politecnico di Milano. His research interests include statistical models for the characterization of interference effects, distributed parameter circuit modeling, experimental procedures and setups for electromagnetic compatibility (EMC) testing, and the EMC in aerospace, automotive, and railway systems. He was a recipient of the EMC Transactions Prize Paper Award, in 2005, the Best Symposium Paper Awards from the Asia–Pacific International Symposium on EMC (APEMC), in 2015, the Richard B. Schulz Best EMC Transactions Paper Award, in 2016, and the Joint IEEE EMC and APEMC Symposium, in 2018.

SERGIO AMEDEO PIGNARI (Fellow, IEEE) received the M.S. and Ph.D. degrees in electronics engineering from the Politecnico di Torino, Turin, Italy, in 1988 and 1993, respectively.

From 1991 to 1998, he was an Assistant Professor with the Department of Electronics, Politecnico di Torino. In 1998, he joined the Politecnico di Milano, Milan, Italy, where he is currently a Full Professor of circuit theory and electromagnetic compatibility (EMC) with the Department of Electronics, Information, and Bioengineering, and the Chair of the board of B.Sc. and M.Sc. degrees study programs in electrical engineering, since 2015. He has authored or coauthored over 200 papers published in international journals and conference proceedings. His research interests are in the field of the EMC and include field-to-wire coupling and crosstalk, conducted immunity and emissions in multi-wire structures, statistical techniques for EMC prediction, and experimental procedures and setups for EMC testing.

Dr. Pignari served as the IEEE EMC Society Chapter Coordinator, from 2010 to 2015. He was a Corecipient of the IEEE EMC Society Technical Achievement Award, in 2011, and the IEEE EMC Society Transactions Prize Paper Award, in 2005 and 2016. From 2007 to 2009, he was the Chair of the IEEE Italy Section EMC Society Chapter. He has been the Technical Program Chair of the ESA Workshop on Aerospace EMC, since 2009, and a member of the Technical Program Committee of the Asia–Pacific EMC Week, since 2010. He has been a member of the International Academic Committee of the State Key Laboratory of Electrical Insulation and Power Equipment (SKLEIPE), Xi'an Jiaotong University (XJTU), Xi'an, China. He is currently serving as an Associate Editor for the IEEE TRANSACTIONS ON ELECTROMAGNETIC COMPATIBILITY.

UMBERTO PAOLETTI (Senior Member, IEEE) received the M.E. degree in electronics engineering from the University of Ancona, Italy, and the Ph.D. degree from the University of Hanover, Germany.

He was with the Fraunhofer Institute for Reliability and Micro Integration, University of Paderborn, Berlin, Germany, and the Graduate School of Engineering, Kyoto University, before joining the Research and Development Group, Hitachi Ltd., Japan, in 2009, where he is currently a Senior Researcher. His research interests include electromagnetics, numerical electromagnetics, measurement techniques for electromagnetic fields, and the EMC at high and low frequencies in all fields and applications. He was a recipient of the Risaburo Sato Award from the International Symposium on Electromagnetic Compatibility, in 2014, and a Corecipient of the Paper Award from the Japan Institute of Electronics Packaging, in 2016.

ISAO HODA (Member, IEEE) received the M.Sc. degree in electrical engineering from Osaka University, Osaka, Japan, in 2000.

He is currently a Senior Researcher with the Research and Development Group, Hitachi Ltd. He has been engaged in the research and development about electromagnetic compatibility (EMC) of automobile electronic components such as an inverter for electrical vehicle or hybrid EV, since 2012. Before then, he had been engaged in the development of a high-frequency circuit for the wireless system and broadcasting receiver for 12 years since he joined Hitachi Ltd., in 2000. He is a member of the Institute of Electrical Engineers (IEE) of Japan and the Institute of Electronics, Information, and Communication Engineers (IEICE) of Japan.